Excitable Front Geometry in Reaction-Diffusion Systems with Anomalous Dispersion

Oliver Steinbock

Florida State University, Department of Chemistry, Tallahassee, Florida 32306-4390

(Received 6 July 2001; published 16 May 2002)

Two-dimensional excitable systems with anomalous dispersion provide a discrete set of interpulse distances for the stable propagation of planar wave trains. Numerical simulations show that the trailing front of a pulse pair can undergo transitions between these stable distances. In response to localized perturbations, the trailing front converges towards one of numerous, sigmoidal shapes. Their transition segments move at constant speeds and can collide and fuse with each other. A complementing kinematic analysis of the front dynamics yields a reaction-diffusion-like equation.

DOI: 10.1103/PhysRevLett.88.228302 PACS numbers: 82.40.Ck, 82.20.Wt, 82.40.Bj

Pattern formation in reaction-diffusion (RD) systems is attracting considerable interest due to its interdisciplinary importance which spans through the entire spectrum of science and engineering [1]. The foremost challenge is to identify steady-state solutions and to derive simple laws that describe their geometrical and dynamic features. In excitable RD media, these solutions include stationary Turing patterns, constant speed and shape pulses, as well as rotating spiral waves [1]. These dissipative structures are observed in a variety of experiments on gas discharge systems, chemical reactions, and living cells [2].

This Letter describes a novel type of steady-state solution which is characteristic for excitable RD systems with anomalous dispersion relations. For planar fronts the dispersion relation denotes the speed (c) of an infinite wave train as a function of the distance between neighboring pulses (λ) [3]. Most of the literature has been dedicated to systems with normal dispersion where $c(\lambda)$ is a monotonic function that increases with λ to asymptotically approach a maximal value which equals the velocity of a solitary pulse c_0 [4]. However, the dispersion relation of excitable systems, in which the steady state is a stable focus, shows either a single overshoot or damped oscillations around c_0 (see Fig. 1a) [5,6]. In the latter case, a discrete spectrum of wavelengths λ_i exists with $c(\lambda_i) = c_0$. At these distances, a leading pulse and a trailing pulse can travel at the same speed. The stability criterion for bound pulse pairs is $dc(\lambda_i)/d\lambda > 0$ [7], which implies that, according to the schematic example in Fig. 1a, stable pulse doublets have distances of λ_0, λ_2, or λ_4.

Experimental studies revealed the existence of anomalous dispersion in a Belousov-Zhabotinsky reaction [8], in the reduction of NO with CO on Pt(100) surfaces [9], and possibly in the aggregation of a cellular slime mold [10]. Furthermore, oscillatory dispersion relations are found in biomedical systems where they influence the propagation of action potentials in cardiac tissue and the nonlinear dynamics of single cardiac cells [11,12]. In this context, the anomaly is often referred to as supernormal excitability. The impact of anomalous dispersion on pattern formation in two spatial dimensions is only sparsely studied [5]. This lack of systematic investigations is in sharp contrast to the highly interesting dynamics one expects to find in this class of excitable systems as we will demonstrate here for the fairly benign example of nonplanar trailing fronts that are frustrated by the existence of multiple stable distances.

Numerical simulations are carried out on the basis of the FitzHugh-Nagumo (FHN) equations [13] which are frequently employed as a generic model for pattern formation in excitable RD systems and neuronal networks:

$$\frac{\partial A}{\partial t} = \frac{1}{\epsilon}(A - A^3/3 - B) + D\nabla^2 A, \tag{1}$$

$$\frac{\partial B}{\partial t} = \epsilon(A + \beta - \gamma B). \tag{2}$$

The dimensionless model involves a fast variable $A(x, y, t)$ and a slow variable $B(x, y, t)$, where x, y, and t denote the spatial coordinates and time, respectively. The parameters are chosen to generate excitable point dynamics around a unique stable focus, which in turn give rise to damped oscillations in the dispersion relation [5].

Figure 2 illustrates the dynamics of a nonplanar excitation front (upper white band) traveling in the wake of a

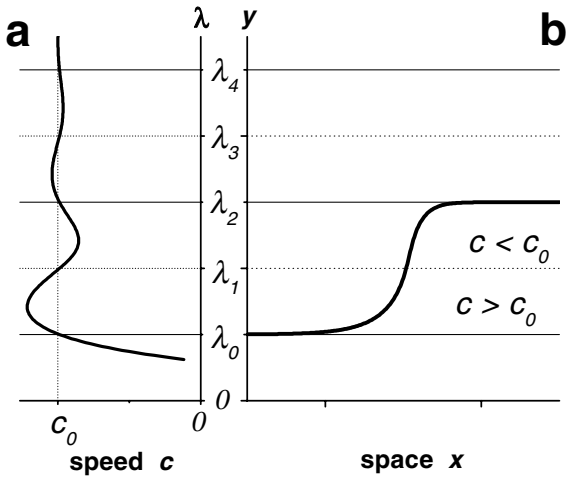

FIG. 1. Schematic drawings of (a) an anomalous dispersion relation with damped oscillations and (b) a defectlike deformation of an excitation front (thick line) that follows a planar front positioned at $y = 0$.

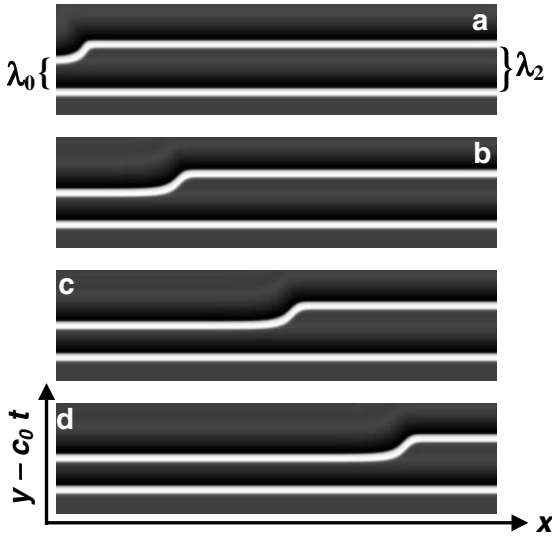

FIG. 2. Four snapshots of a pair of excitation fronts (white bands) in a moving coordinate system $(x, y - c_0 t)$. The parameters ϵ, β, γ, and D are 0.3, 0.7, 0.5, and 1.0, respectively. The numerical integration is carried out with a time step of $\Delta t = 0.01$ on a grid of 400×100 points spaced at $\Delta x = 0.5$.

planar pulse (lower white band). The consecutive snapshots 2(a)–2(d) are taken in a coordinate system $y - c_0 t$ that moves with the speed of the leading front in the $-y$ direction. The initial geometry of the trailing pulse is chosen in a way that a small portion of its front is spaced from the predecessor at a distance λ_0 while the spacing of the longer, right portion is λ_2. Both of these distances are stable with respect to perfectly planar fronts but the connecting, curved segment extends through an area in which the local pulse speed varies around c_0 (compare Fig. 1b). Our simulations reveal that the trailing front quickly establishes a steady-state shape that propagates with constant speed in the x direction. Most of the front is locked into one of the stable positions, and the curved transition zone is, hence, well localized. The direction of its motion leads to an expansion of the λ_0 segment at the expense of the λ_2 branch. We will therefore denote this structure as the $+(\lambda_2 \rightarrow \lambda_0)$ transition where the plus sign indicates the direction of the traveling transition zone with respect to the x axis. Attempts to initiate the reverse transition from λ_0 to λ_2 were always unsuccessful. Note that we found no indications for a dependence between the features of the transition shown in Fig. 2 and the detailed shape of the initial perturbation. However, the amplitude and the width of the initial deformation has to exceed critical values in order to nucleate the traveling structure. All of these findings suggest that the moving front deformation shown in Fig. 2 is indeed a novel steady-state solution of excitable RD systems revealing intriguing similarities to the nucleation and propagation of fronts in bistable systems [14].

The existence of several stable distances in the wake of the leading pulse allows the formation of additional transitions along the trailing front. Figure 3a presents an example of a traveling $+(\lambda_4 \rightarrow \lambda_2)$ transition. The corresponding transition zone is smoother than the one shown in Fig. 2 and moves at a slower speed. This difference in propagation velocities creates the possibility for collisions between $(\lambda_4 \rightarrow \lambda_2)$ and $(\lambda_2 \rightarrow \lambda_0)$ transitions as illustrated by the image sequence in Fig. 3. In the collision a constant-shape $+(\lambda_4 \rightarrow \lambda_0)$ pattern is formed that continues to propagate towards the right (Fig. 4d). The velocity of this newly formed structure shows no significant difference from that of the $(\lambda_2 \rightarrow \lambda_0)$ transition.

According to the number of stable distances N on the dispersion curve, it is possible to observe $N^2 - N$ different, nontrivial steady-state solutions. The resulting, large number of allowed (i.e., topologically possible) collisions can be categorized into two main classes. A collision occurs either by front-to-back fusion, as shown in Fig. 3, or in front-to-front encounters that lead to complete or partial annihilation. An example for the latter case is shown in the image sequence of Fig. 4. Here a $+(\lambda_4 \rightarrow \lambda_0)$ transition collides with a $-(\lambda_4 \rightarrow \lambda_2)$ zone giving birth to a rightwards traveling $+(\lambda_2 \rightarrow \lambda_0)$ structure (Fig. 4d) that will eventually generate a planar front at the stable distance λ_0 (not shown).

In the following, we present a simple kinematic analysis of the above front dynamics which reproduces the essential findings of our simulations and explains the surprising similarity between the steady evolution of the front shape and the constant-speed propagation of fronts in multistable systems. The position y_L of the leading planar front is described by $y_L(t) = c_0 t$. It generates a spatially modulated, steadily translating velocity field that affects the evolution of the trailing front $y(x, t)$. The local curvature K of the trailing front $y(x, t)$ is essential for the formation of a steady-state solution. The curvature influences the normal

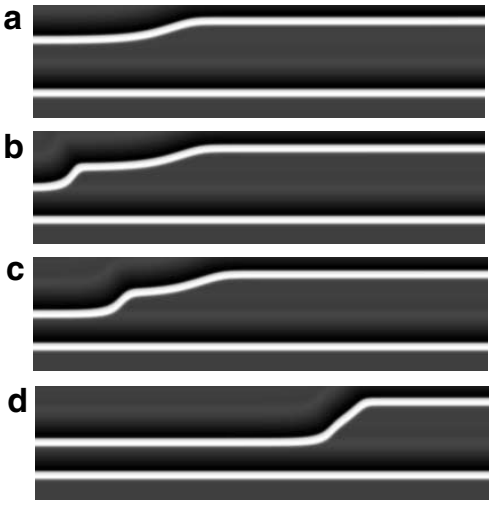

FIG. 3. Front-to-back collision of a $+(\lambda_2 \rightarrow \lambda_0)$ with a $+(\lambda_4 \rightarrow \lambda_2)$ transition. This type of collision generates a $+(\lambda_4 \rightarrow \lambda_0)$ transition. Numerical parameters as in Fig. 2.

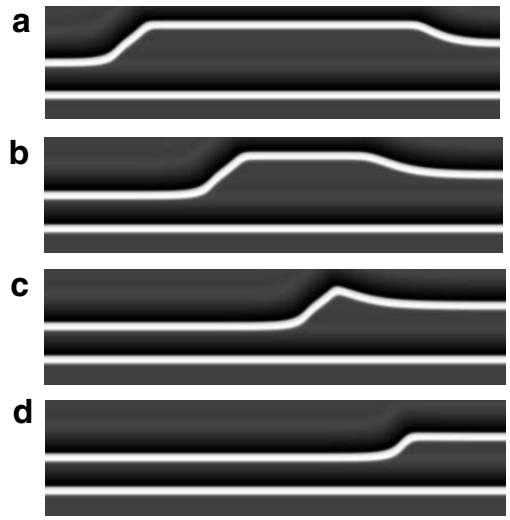

FIG. 4. Front-to-front collision of a $+(\lambda_4 \rightarrow \lambda_0)$ with a $-(\lambda_4 \rightarrow \lambda_2)$ transition. This collision results in the formation of a $+(\lambda_2 \rightarrow \lambda_0)$ structure. Numerical parameters as in Fig. 2.

front velocity N according to the eikonal equation, which, with respect to a planar pulse, yields increased (decreased) speeds for concave (convex) front segments [15]. This dependence stabilizes the trailing pulse which experiences a continuous deformation from the modulated velocity field and can be written as

$$N = \begin{pmatrix} N_x \\ N_y \end{pmatrix} = \frac{c + DK}{\sqrt{1 + (\partial y/\partial x)^2}} \begin{pmatrix} -\partial y/\partial x \\ 1 \end{pmatrix}, \quad (3)$$

where $1/\sqrt{1 + (\partial y/\partial x)^2}$ times the following vector is the unit vector in normal direction. Note that c is the position-dependent wave speed of a planar front (compare Fig. 1). From the equations

$$\partial y/\partial t = N_y - N_x \partial y/\partial x\,, \quad (4)$$

$$K = (\partial^2 y/\partial x^2)/[1 + (\partial y/\partial x)^2]^{3/2}\,, \quad (5)$$

one readily obtains the kinematic equation

$$\frac{\partial \overline{y}}{\partial t} = -c_0 + \xi c(\overline{y}) + \frac{D}{\xi^2}\frac{\partial^2 \overline{y}}{\partial x^2}\,, \quad (6)$$

where $\xi = \sqrt{1 + (\partial \overline{y}/\partial x)^2} \geq 1$ is the derivative of the arclength with respect to x and $\overline{y}$ equals $y - c_0 t$. The main structure of Eq. (6) is reminiscent of a one-dimensional RD system [14]. However, ξ can locally amplify the oscillatory "reaction term" $c(y)$ and weaken the stabilizing diffusion-like term in (6). For oscillatory dispersion relations, the spatially homogeneous steady states of Eq. (6) correspond to planar waves ($\xi = 1$) with $\overline{y}(x) = \lambda_0, \lambda_2, \ldots$. For systems with normal dispersion, the equation still holds but yields no stationary solutions.

Figure 5 shows numerical results obtained on the basis of Eq. (6) for the simple model dispersion relation $c(\overline{y}) = c_0 + c_1 \sin(k\overline{y})$. In this example, the wave vector k is set to $2\pi/4.0$ and homogeneous steady states are found accordingly at $\overline{y} = 2.0, 6.0, 10.0, \ldots$. The bold curve in

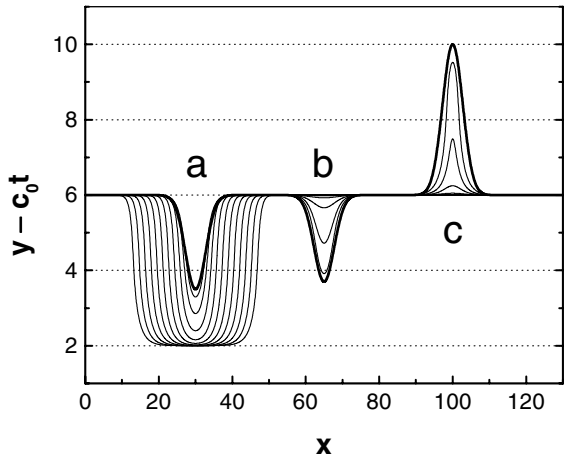

FIG. 5. Front evolution obtained by numerical integration of Eq. (6) for a sinusoidal dispersion relation without damping. The thick line indicates the initial condition which involves three localized perturbations (a)–(c) of the stationary solution $y = 6.0$. Only perturbation (a) succeeds in initiating a pair of traveling transition zones. Parameters: $c_0 = -2.0$, $c_1 = 0.5$, $k = 2\pi/4.0$, $D = 1.0$.

Fig. 5 represents the initial shape of $\overline{y}(x)$ which is a straight line at $\overline{y} = 6.0$ perturbed by three bell-shaped curves [labeled (a)–(c)] of different amplitude. The 11 additional curves are illustrating the consecutive front evolution. The perturbation 5(a) extends into the band of high propagation speeds between $\overline{y} = 2$ and 4. In the course of time, this leading segment decreases its distance from the attractive position at $\overline{y} = 2$, and two propagating $(\lambda_2 \rightarrow \lambda_0)$ transition fronts are formed that travel at a constant speed in opposite directions. The second perturbation 5(b) has a slightly smaller amplitude. Again, this perturbation is large enough to extend the initial front into the band of increased propagation speeds, but, in this case, the front reclines towards larger $\overline{y}$ values and no defect nucleation is observed. This behavior is caused by the negative curvature of the convex, leading segment, which in this example is sufficiently strong to overcompensate the elevated speeds below $\overline{y} = 4.0$. The third perturbation 5(c) deforms the planar front in the opposite direction and collapses rapidly into the stable $\overline{y} = 6.0$ state.

The overall dynamics represented in Fig. 5 are in good qualitative agreement with the behavior of fronts in our FHN simulations. In the framework of the simple dispersion relation used for Fig. 5, one finds that the propagation velocity of the defects increases with increasing values of the modulation amplitude c_1. This increase in speed coincides with a decrease of the defect's half-width. A major difference, however, is that the defect speed is independent from the specific transition because the oscillations of the dispersion relations are not damped. A straightforward modification of our earlier dispersion relation is $c(\overline{y}) = c_0 + c_1 \sin(k\overline{y}) \exp(-\kappa\overline{y})$. Figure 6 shows a time-space plot obtained by numerical integration of Eq. (6) using the latter velocity expression. In this plot,

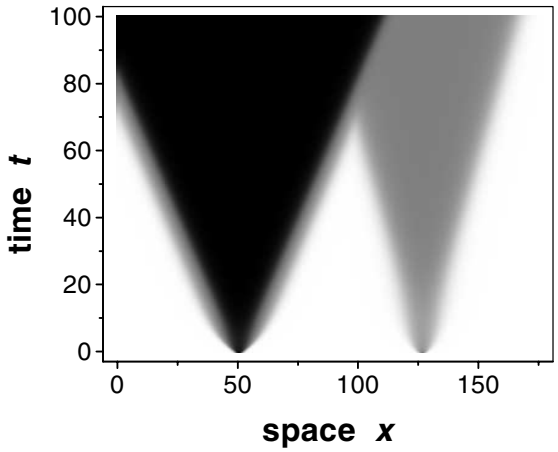

FIG. 6. Time-space plot obtained on the basis of Eq. (6) for a dispersion relation with exponentially damped sinusoidal oscillations. The local gray levels represent the corresponding value of $\overline{y}(x,t)$ with black indicating $y = \lambda_0$. Parameters as in Fig. 5 and $\kappa = 0.3$.

different gray levels indicate different distance between the leading and trailing fronts. The dominant halftones represent $\overline{y} = \lambda_0$ (black), λ_2 (gray), and λ_4 (white). For this example, an initial state $\overline{y}(x) = \lambda_4$ is perturbed to nucleate pairs of $(\lambda_4 \rightarrow \lambda_0)$ and $(\lambda_4 \rightarrow \lambda_2)$ transitions. The data in Fig. 6 clearly show that the $(\lambda_4 \rightarrow \lambda_0)$ zones travel at a higher speed than the $(\lambda_4 \rightarrow \lambda_2)$ transition, whereas the speed of the $(\lambda_4 \rightarrow \lambda_0)$ and $(\lambda_2 \rightarrow \lambda_0)$ transitions are identical. These findings are in good agreement with the FHN simulations, which indicate that the particle-like dynamics of the front deformations are indeed caused by the interplay of the destabilizing velocity variations and the stabilizing effect of front curvature.

In conclusion, this study revealed a novel class of steady-state solutions in excitable RD systems. These solutions are particle-like, traveling front deformations that mediate transitions within stable bound pulse pairs. They are characteristic for all wave-supporting media in which the steady state is a stable focus. Accordingly, we expect that the phenomena described should exist in a broad variety of physicochemical and biological systems.

The author thanks Robert L. Fulton for discussions.

[1] *Chemical Waves and Patterns,* edited by R. Kapral and K. Showalter (Kluwer, Dordrecht, The Netherlands, 1995).
[2] Y. Astrov, E. Ammelt, S. Teperick, and H. G. K. Purwins, Phys. Lett. A **211**, 184 (1996); K. Agladze and O. Steinbock, J. Phys. Chem. A **104**, 9816 (2000); Y. Nagai, H. Gonzalez, A. Shrier, and L. Glass, Phys. Rev. Lett. **84**, 4248 (2000).
[3] C. Elphick, E. Meron, and E. A. Spiegel, Phys. Rev. Lett. **61**, 496 (1988); C. Elphick, E. Meron, and E. A. Spiegel, SIAM J. Appl. Math. **50**, 490 (1990); C. Elphick, E. Meron, J. Rinzel, and E. A. Spiegel, J. Theor. Biol. **146**, 249 (1990).
[4] J. M. Flesselles, A. Belmonte, and V. Gaspar, J. Chem. Soc. Faraday Trans. **94**, 851 (1998).
[5] A. T. Winfree, Phys. Lett. **149**, 203 (1990); A. T. Winfree, Physica (Amsterdam) **49D**, 125 (1991).
[6] M. Or-Guil, I. G. Kevrekidis, and M. Bär, Physica (Amsterdam) **135D**, 154 (2000); M. G. Zimmermann *et al.,* Physica (Amsterdam) **110D**, 92 (1997).
[7] J. Rinzel and K. Maginu, in *Nonequilibrium Dynamics in Chemical Systems,* edited by C. Vidal and A. Pacault (Springer, Berlin, 1984), pp. 107–113.
[8] C. T. Hamik, N. Manz, and O. Steinbock, J. Phys. Chem. A **105**, 6144 (2001); C. T. Hamik and O. Steinbock, Phys. Rev. E **65**, 046224 (2002).
[9] J. Christoph *et al.,* Phys. Rev. Lett. **82**, 1586 (1999).
[10] F. Siegert and C. J. Weijer, J. Cell Sci. **93**, 325 (1989).
[11] J. D. Kocsis, H. A. Sawdlow, S. G. Waxman, and M. H. Brill, Exp. Neurol. **65**, 230 (1979).
[12] D. R. Chialvo, R. F. Gilmour, and J. Jalife, Nature (London) **343**, 653 (1990); D. R. Chialvo, D. C. Michaels, and J. Jalife, Circ. Res. **66**, 525 (1990); A. Vinet, D. R. Chialvo, D. C. Michaels, and J. Jalife, Circ. Res. **67**, 1510 (1990).
[13] R. Fitzhugh, Biophys. J. **1**, 445 (1961).
[14] R. D. Benguria and M. C. Depassier, Phys. Rev. Lett. **77**, 1171 (1996); P. C. Fife, *Mathematical Aspects of Reacting and Diffusing Systems*, Lecture Notes in Biomathematics Vol. 28 (Springer-Verlag, New York, 1979).
[15] A. S. Mikhailov, *Foundations of Synergetics I* (Springer-Verlag, Berlin, 1990); V. A. Davydov, V. S. Zykov, and A. S. Mikhailov, Usp. Fiz. Nauk **161**, 45 (1991); J. J. Tyson and J. P. Keener, Physica (Amsterdam) **32D**, 327 (1988).